Biosensors and Bioelectronics 134 (2019) 8–15

Contents lists available at ScienceDirect

Biosensors and Bioelectronics

journal homepage: www.elsevier.com/locate/bios

Bimetallic ZrHf-based metal-organic framework embedded with carbon dots: Ultra-sensitive platform for early diagnosis of HER2 and HER2-overexpressed living cancer cells

Chenxi Gu[a], Chuanpan Guo[b], Zhenzhen Li[b], Minghua Wang[b], Nan Zhou[a,*], Linghao He[b], Zhihong Zhang[b,*], Miao Du[b,*]

[a] Department of Orthopedics, The First Affiliated Hospital of Zhengzhou University, Zhengzhou 450052, PR China
[b] Henan Provincial Key Laboratory of Surface and Interface Science, Zhengzhou University of Light Industry, Zhengzhou 450002, PR China

ARTICLE INFO

Keywords:
ZrHf-based metal–organic framework
Electrochemical aptasensor
Early diagnosis of HER2
Detection of MCF-7 cells

ABSTRACT

We report here a new bimetallic ZrHf metal–organic framework (ZrHf-MOF) embedded with abundant carbon dots (CDs) (denoted as CDs@ZrHf-MOF), which exhibits strong fluorescence and rich-amino-functionalization. The CDs@ZrHf-MOF can be applied as the scaffold for anchoring aptamer strands to determine human epidermal growth factor receptor-2 (HER2) and living HER2-overexpressed MCF-7 cells. The basic characterizations reveal that the CDs are embedded within the interior cavities of ZrHf-MOF without varying the nanostructure, leading to good biocompatibility, strong fluorescence, and high electrochemical activity of CDs@ZrHf-MOF. As compared with the pristine ZrHf-MOF, the CDs@ZrHf-MOF-based electrochemical aptasensor displays better sensing performances toward both HER-2 and MCF-7 cells, giving an extremely low detection limit of 19 fg mL^{-1} (HER2 concentration range: 0.001–10 ng mL^{-1}) and 23 cell mL^{-1} (cell concentration range: 1×10^2~1×10^5 cell mL^{-1}), with good selectivity, stability, reproducibility, and acceptable applicability. The proposed strategy for developing CDs@ZrHf-MOF-based aptasensor is promising for the early and sensitive detection of cancer markers and living cancer cells.

1. Introduction

Nowadays, the increase of diseases, especially cancers, is a major global concern. Among different cancers, breast cancer is one of the most common malignancies and diagnosed cancers in women (DeSantis et al., 2015). More than 90% of these deaths are related to metastatic growth. Therefore, early stage detection of cancer is crucial to increase the chances of survival. Human epidermal growth factor receptor 2 (HER2) protein, a transmembrane tyrosine kinase receptor and a member of the epidermal growth factor receptors (EGFR or ErbB) family, is overexpressed in breast, ovarian, lung, gastric, and oral cancers (Ilkhani et al., 2015; Vivek et al., 2014). Breast cancer patients possess high HER2 concentrations in their blood (14–75 ng mL^{-1}) compared to normal individuals (4–14 ng mL^{-1}) and can be utilized for diagnosis and active surveillance of patients at risk or in treatment (Arya et al., 2018). Currently, various HER2 detection techniques have been reported, including immunohistochemical assays (Arkan et al., 2015; Bethune et al., 2015), enzyme-linked immunosorbent assay (Furrer et al., 2015), surface enhanced Raman scattering (Téllez-Plancarte et al., 2018), fluorescence (Chinen et al., 2015), electrochemiluminescence (Emami et al., 2014; Ravalli et al., 2016), and electrochemical techniques (Ilkhani et al., 2016). However, most of these techniques require sophisticated instrumentation, special training and are labor-intensive and time-consuming. In this context, the electrochemical detection technique has attracted great attention for its simple equipment and high sensitivity (Ju and Chen, 2015).

Aptamers, single strand oligonucleotides (DNAs or RNAs) that are designed and developed synthetically in the laboratory, display highly specificity to bind with various targets, such as proteins (Toh et al., 2015), circulating tumor cells (CTCs) (Shan et al., 2018), circulating tumor DNA (ctDNA) (Ilkhani and Farhad, 2018; Li et al., 2018a), and exosomes (Dong et al., 2018). Their prominent properties including good thermal and chemical stability, low cost, high reusability, and easy modification enable them to become a perfect tool in biosensor applications and disease diagnosis (Bala et al., 2016). Thereby, combining electrochemical techniques with the overwhelming aptamers, the electrochemical aptasensors are particularly suitable for constructing rapid, sensitive, miniaturized, and on-site testing platforms.

* Corresponding authors.
E-mail addresses: fcczhoun@zzu.edu.cn (N. Zhou), 2006025@zzuli.edu.cn (Z. Zhang), dumiao@zzuli.edu.cn (M. Du).

https://doi.org/10.1016/j.bios.2019.03.043
Received 17 January 2019; Received in revised form 3 March 2019; Accepted 20 March 2019
Available online 22 March 2019
0956-5663/

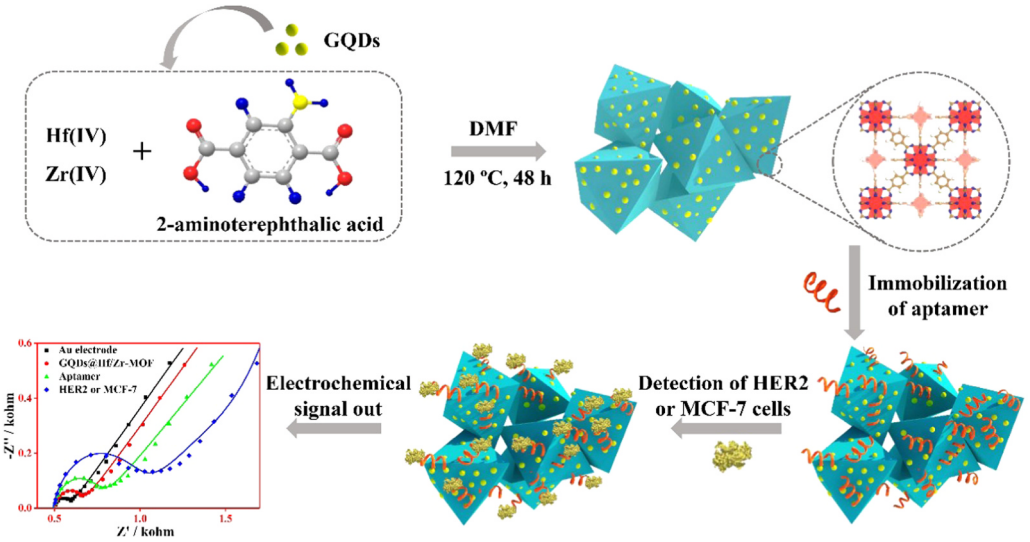

Scheme 1. Schematic diagram of the fabrication procedure of CDs@ZrHf-MOF-based aptasensor for detecting HER2: (i) the preparation of the series of CDs@ZrHf-MOF composites, (ii) the immobilization of the aptamer strands, and (iii) the HER2 detection using the proposed CDs@ZrHf-MOF-based aptasensor.

Various electrochemical biosensors for detecting HER2 have been developed based on different nanomaterials, such as the rGO-chit composite (Tabasi et al., 2017), thiol terminated DNA aptamer (Arya et al., 2018), and bimetallic MnFe Prussian blue analogue (Zhou et al., 2019). Additionally, aside from the sensitive determination of cancer markers by electrochemical techniques, the living cancer cells also can be detected using electrochemical aptasensors (Zhang et al., 2018). Since the density of cancer cells in peripheral bloodies is relatively lower, early stage determination still remains a major challenge and it is urgently desired to develop a fast, cost effective, specific and ultrasensitive method for monitoring cancer (Ye et al., 2015). Also, the simultaneous detection of cancer markers and living cells by electrochemical techniques has been seldom reported, because the sensitive layer therein needs to meet the requirements of both electrochemical activity and fluorescence performance. Very recently, a porphyrin-based covalent–organic framework has been exploited as a bifunctional sensing layer for detecting trace EGFR and living michigan cancer foundation-7 (MCF-7) (Yan et al., 2019). Nevertheless, it is still necessary to develop feasible biosensors with the comprehensive properties for detecting biomarkers and cancer cells.

Metal–organic frameworks (MOFs) have emerged over the past two decades with the potentials to act as promising materials in gas storage, chemical separation, catalyst, magnetism, sensing, and drug delivery etc (Du et al., 2013; Zhou and Kitagawa, 2014). Additionally, the secondary interactions, such as π–π stacking, hydrogen bonding, and electrostatic force, can be formed between special functional groups on MOFs linkers and negatively charged nucleic acid sequences (Liu et al., 2017b; Zhang et al., 2017a). Thus, a series of MOFs-based biosensors have been designed to detect various targeted analytes, such as MOF/Au/G-quadruplex (Shao et al., 2018), zinc-methylimidazolate framework-8 (Pan et al., 2018), and NH_2-Ni-MOF (Wang et al., 2018b). Although several kinds of MOFs have been explored to determine H_2O_2 released from living cells by electrochemical methods (Li et al., 2018a), the direct detection of living cancer cells has not been achieved. Consequently, it would be highly desirable to explore MOFs-based scaffolds for simultaneously detection of HER2 and living cancer cells. In the previous work, bimetallic MnFe Prussian blue analogue coupled to gold nanoparticles has been developed for the determination of HER2 and living MCF-7 cells, only giving a limitation of detection of 0.247 pg mL^{-1} and 36 cell mL^{-1} toward HER2 and MCF-7 cells, respectively (Zhou et al., 2019). Lately, many synthetic efforts toward MOFs have focused on those with group IV transition metal ions, especially zirconium and hafnium (Takata et al., 2015). Zr and Hf MOFs with linear dicarboxylate ligands generally adopt the well documented UiO-66 topology, where $M_6O_4(OH)_4$ clusters (M = Zr or Hf) are linked in three dimensions by bridging organic ligands (Morris et al., 2017). In virtue of the excellent biocompatibility, chemical stability, strong bioaffinity, and high binding interactions of Zr–O–P between MOF frameworks and DNA strands (Chen et al., 2016), some Zr-MOF-based aptasensors have been fabricated to sensitively determine different analytes (Guo et al., 2017; Liu et al., 2018), and UiO-66-N_3 to create the first MOF nanoparticle-nucleic acid conjugates (Morris et al., 2014). Nevertheless, most Zr-MOFs suffer from their poor electrochemical activity (Vermoortele et al., 2013), thus limiting the applications in electrochemical biosensors.

Owing to their high surface areas, tunable pore sizes, and excellent adsorbability, MOFs could be served as effective solid multifunctional matrixes for other components, such as metal nanoparticles (Duan et al., 2018), metal oxide NPs (Falcaro et al., 2016), and quantum dots (Zhao et al., 2014). Among them, carbon dots (CDs), as carbon-based photoluminescent nanomaterials (< 10 nm in size), may show great potentials in developing sensitive, stable, and cost-effective aptasensor (Zhang et al., 2017b). Further, CDs can be applied to enhance the immobilization of aptamer probes, with the exception of their hydrophobicity, chemical stability, electro-conductivity, biocompatibility, cost efficiency, and easy synthesis (Tuteja et al., 2016). Based on the above analysis, aiming at developing a novel bifunctional electrochemical aptasensor for simultaneously detecting HER2 and living cancer cells (MCF-7), we have prepared a bimetallic ZrHf-MOF coupling with CDs (represented by CDs@ZrHf-MOF) and explored it as the scaffold for anchoring HER2 aptamer (Scheme 1). Combining the advantages of large specific area, high stability, strong bioaffinity toward biomolecules, and excellent biocompatibility of ZrHf-MOF and good fluorescence, high electrochemical activity, and outstanding biosensing performance of CDs (Wang et al., 2015), the fabricated CDs@ZrHf-MOF-based electrochemical aptasensor not only can be applied to sensitively detect the trace HER2 in human serum sample, but also can determine the living cancer cells. The electrochemical CDs@ZrHf-MOF-based aptasensor displays extremely low limitation of detections (LODs) of 19 fg mL^{-1} toward HER2 and 23 cell mL^{-1} for MCF-7 cells, also with good selectivity, stability, reproducibility, and acceptable applicability. This work could supply a promising approach for early diagnosis of both cancer marker and living cancer cells.

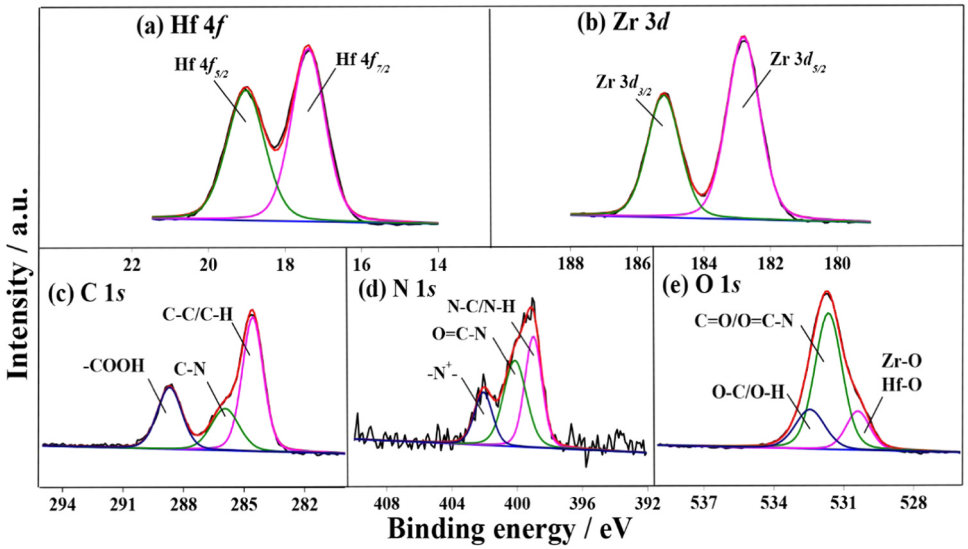

Fig. 1. (a) Hf 4*f*, (b) Zr 3*d*, (c) C 1*s*, (d) N 1*s*, and (e) O 1*s* core-level XPS spectra of CDs@ZrHf-MOF.

2. Experimental section

The parts of chemicals and regents, preparation of solutions, pretreatment of the bare Au electrode, cell culture, cytotoxicity in vitro, cell imaging, characterizations, and electrochemical measurements are supplied in the S1 (See the Supplementary Information). The preparation procedures of Hf-MOF, Zr-MOF, ZrHf-MOF, and CDs are supplied in S1.2 and 1.3.

2.1. Preparation of CDs@ZrHf-MOF

The CDs solution (4 mL) was added into a mixed solution of $HfCl_4$ (147 mg, 0.46 mmol) and $ZrCl_4$ (107 mg, 0.46 mmol). After homogeneous mixing, 2-aminoterephthalic acid (84 mg, 0.46 mmol), formic acid (1.5 mL), and dimethylformamide (38.5 mL) were added to the above suspension. Then, the mixture was moved into an autoclave vessel and heated at 120 °C for 48 h. Subsequently, the product was filtered and washed with an excess of DMF and ethanol.

2.2. Fabrication of the electrochemical aptasensors

In the present work, four kinds of aptasensors based on Hf-MOF, Zr-MOF, ZrHf-MOF, and CDs@ZrHf-MOF were developed. Taking the CDs@ZrHf-MOF-based aptasensor as an example, 1.0 mg CDs@ZrHf-MOF powder was dispersed in 1.0 mL of Milli-Q water, followed by ultrasonically agitating for 30 min to form a homogeneous suspension. Afterward, 5.0 μL of aqueous CDs@ZrHf-MOF suspension (1.0 mg mL^{-1}) was dropped onto the pre-treated Au electrode (AE) surface, followed by being dried with ultrapure N_2. Subsequently, CDs@ZrHf-MOF/AE was incubated with the HER2 aptamer solution to anchor the aptamer strands (denoted as Apt/CDs@ZrHf-MOF/AE). As such, the developed Apt/CDs@ZrHf-MOF/AE aptasensor was obtained and used for further electrochemical measurements. For comparison, aptasensors based on Hf-MOF, Zr-MOF, and ZrHf-MOF were similarly developed. All aptasensors were stored at 4 °C in a refrigerator when not in use.

3. Results and discussion

3.1. Working mechanism of the CDs@ZrHf-MOF-based aptasensor toward HER2 and MCF-7 cells

Because the HER2 aptamer strand, 5′-GGG CCG TCG AAC ACG AGC ATG GTG CGT GGA CCT AGG ATG ACC TGA GTA CTG TCC-3′ (Niazi et al., 2015), is composed of 54 mer bases, it is hard to stably adsorb over the MOF surface, further leading to release of the formed G-quadruplex coordination. Thus, it is crucial to optimize the sensitive layer for biosensors to immobilize the aptamer strand and stabilize the formed G-quadruplex. Given the strong bioaffinity and intrinsic porosity of CDs@ZrHf-MOF (Wang et al., 2015), it may serve as a good scaffold for immobilizing HER2 aptamer strands, followed by the recognition toward HER2 via forming G-quadruplex between aptamer strands and HER2 (Tabasi et al., 2017). Furthermore, living MCF-7 cells can release the HER2 marker, and a clear electrochemical signal can also be obtained when the CDs@ZrHf-MOF-based aptasensor is in contact with MCF-7 cells. Electrochemical techniques were applied to estimate each step during the detection procedure of HER2 and living MCF-7 cells by aptasensor based on CDs@ZrHf-MOF.

3.2. Basic characterizations of CDs, MOFs, and CDs@ZrHf-MOF

The as-synthesized CDs were characterized via TEM, UV–vis absorption spectroscopy, fluorescent spectroscopy, and X-ray photoelectron spectroscopy (XPS) (Figs. S1 and S2). All results hint the successful preparation of CDs (See S2 in the Supplementary Information).

Surface morphologies of Zr-MOF, Hf-MOF, ZrHf-MOF, and CDs@ZrHf-MOF were investigated by TEM (See S3 in the Supplementary Information). The HR-TEM image of CDs@ZrHf-MOF illustrates a lattice of 0.213 nm, which is corresponded to the (100) diffraction plane of sp^2 graphitic carbon, implying the presence of CDs. The chemical structure and component were revealed by Fourier transform infrared (FT-IR) and XPS spectra, whereas the crystal nanostructure was evaluated by XRD pattern (See S4 in the Supplementary Information). The high-resolution XPS of each element of CDs@ZrHf-MOF and ZrHf-MOF indicates the similar results of Hf 4*f*, Zr 3*d*, C 1*s*, and O 1*s* (Fig. 1 and S8). Two peaks of Zr $3d_{3/2}$ and Zr $3d_{5/2}$ are found for the two samples, along with Hf $4f_{5/2}$ and Hf $4f_{7/2}$, hinting the coexistence of Zr and Hf elements. Also, the Hf–O and Zr–O groups are found in the high-resolution O 1*s* spectrum. Compared with the ZrHf-MOF, an additional peak at 401 eV is deconvoluted for the high-resolution N 1*s* XPS spectrum of CDs@ZrHf-MOF, which is corresponded to the $-N^+-$ group formed by protonation of $-NH_2$. This feature would facilitate the aptamer strand immobilization via the electrostatic interactions between the $-N^+-$ groups and the phosphates of aptamer strands (Zhang et al., 2015).

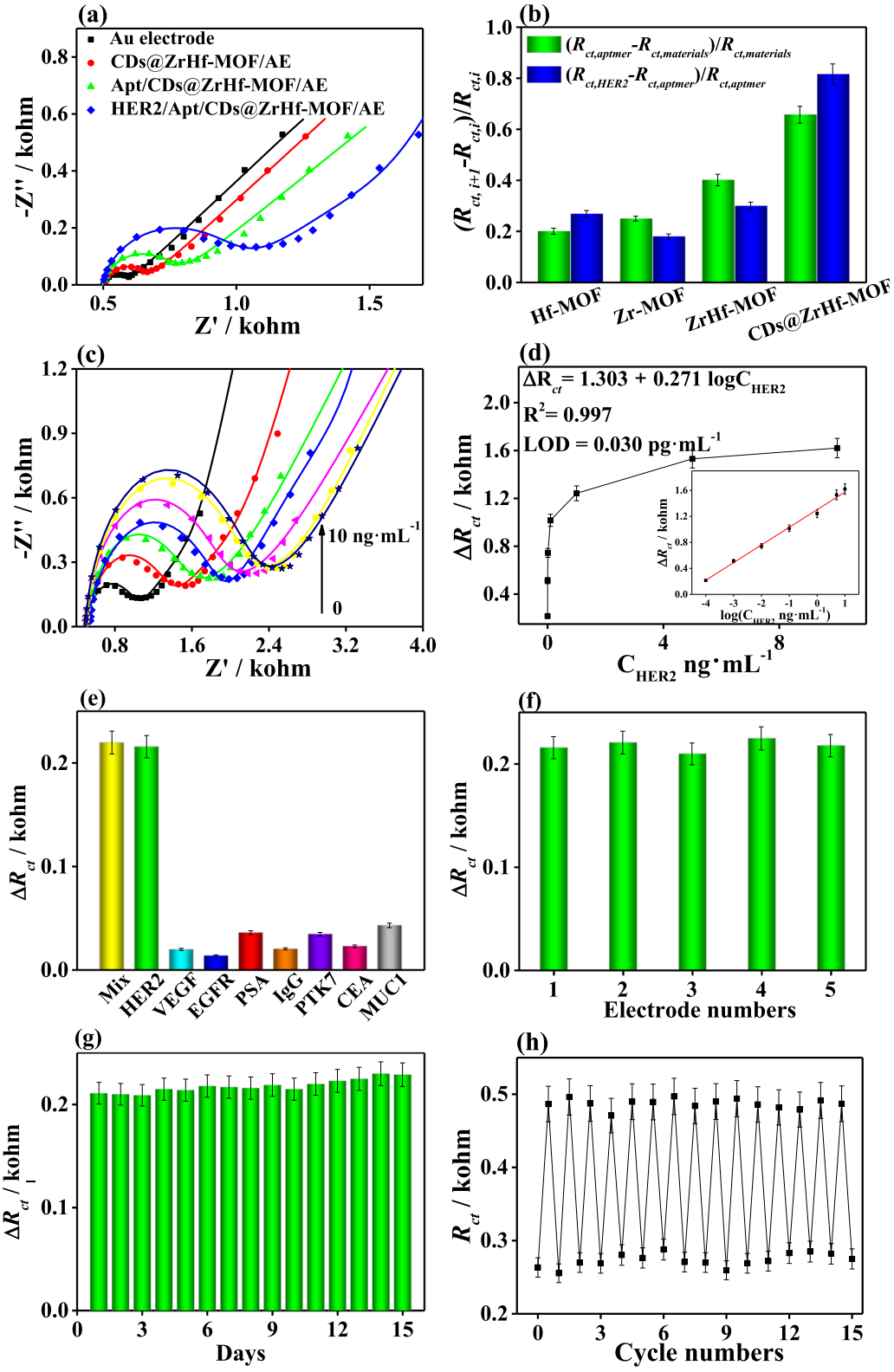

Fig. 2. (a) EIS Nyquist plots of CDs@ZrHf-MOF-modified AE for the detection of 0.0001 ng mL^{-1} HER2. (b) Variation in the charge-transfer resistance (R_{ct}) values for each stage in HER2 detection. (c) EIS responses of the CDs@ZrHf-MOF/AE with different HER2 concentrations (0, 0.0001, 0.001, 0.01, 0.1, 1, 5, and 10 ng mL^{-1}). (d) Dependence of ΔR_{ct} on the concentration of HER2 (inset: the linear parts of calibration curves). (e) ΔR_{ct} values of CDs@ZrHf-MOF-based electrochemical aptasensor by separately adding the interferences (VEGF, EGFR, PSA, IgG, PTK7, CEA, and MUC1 with the concentration of 0.01 ng·mL^{-1}), HER2 (0.1 pg mL^{-1}), and their mixture. (f) Reproducibility of the CDs@ZrHf-MOF-based aptasensor for detecting HER2 with the concentration of 0.1 pg mL^{-1}. (g) Stability of the CDs@ZrHf-MOF-based electrochemical aptasensor for detecting HER2 (0.1 pg mL^{-1}) within 15 days. (h) Regenerability of the CDs@ZrHf-MOF-based aptasensor for detecting HER2 with the concentration of 0. 1 pg mL^{-1}.

3.3. Electrochemical performances of MOFs and CDs@ZrHf-MOF

EIS technique is effective and convenient to investigate the variation for each step during the fabrication of electrochemical biosensor (Guo et al., 2017). The correlation parameters for EIS Nyquist plots were obtained by using the Randles equivalent circuit to calculate the experimental data. As shown in Fig. 2a inset, a modified Randles equivalent circuit is composed of a resistance of the electrolyte solution (R_s), Warburg diffusion impedance (W_o) (Bagheri et al., 2016), double-layer capacitance (Feng et al., 2010) (CPE), and the electron-transfer resistance (R_{ct}). Notably, R_{ct} is important to control the electron transfer kinetics of the redox probe at the electrode interface. The CDs@ZrHf-MOF was explored as the sensitive layer for the aptamer immobilization to detect HER2 (Fig. 2a). The bare AE shows a small semicircle at the high frequency with a small R_{ct} value, 0.092 kohm, suggesting a fast electron-transfer process (Guo et al., 2017). When the AE was modified

by CDs@ZrHf-MOF (denoted as CDs@ZrHf-MOF/AE), the R_{ct} value would increase to 0.159 kohm, indicating a slower electron-transfer. However, in comparison with other monometallic or bimetallic MOFs [e.g. Zr-MOF R_{ct} = 1.23 kohm (Guo et al., 2017), Al-MOF R_{ct} = 1.80 kohm (Liu et al., 2017a), Ce/Cu-MOF R_{ct} = 0.53 kohm (Wang et al., 2019), CuFe PBA R_{ct} = 0.28 kohm (Zhou et al., 2018)], the R_{ct} value of the CDs@ZrHf-MOF-modified electrode is much smaller, hinting the relative higher electrochemical activity due to the incorporation of CDs. When the aptamer strands are immobilized on the surface of CDs@ZrHf-MOF/AE, the R_{ct} value slightly increases to 0.261 kohm. In the water solution, the phosphate groups in aptamer strands would ionized into abundant negative charges, which can inhibit the electron transfer at the electrode surface owing to the strong electrostatic repulsion with $[Fe(CN)_6]^{3-/4-}$ redox couple (Wang et al., 2018a). As such, it results in a large R_{ct} for the EIS response. When the CDs@ZrHf-MOF-based aptasensor was used to detect HER2, the interactions between aptamer strands and HER2 would lead to the formation of aptamer/HER2 complex via opening the hairpin of the long HER2 aptamer (Tabasi et al., 2017), further leading to the increase of R_{ct} value (0.480 kohm). Simultaneously, CV and DPV measurements were also taken to investigate the fabrication procedure of the CDs@ZrHf-MOF-based aptasensor (Fig. S10), in which similar results are observed (See S6 in the Supplementary Information).

For comparison, Hf-MOF, Zr-MOF, and ZrHf-MOF were also applied respectively for the construction of aptasensors (Fig. S11). Similar trends were obtained, including the modification with different MOFs, the aptamer immobilization, and the HER2 detection. In order to minimize the variability among these aptasensors, the relative variation in R_{ct} ($\Delta R_{ct}/R_{ct}$) was used to evaluate their sensing performances (Golabi et al., 2017). The $\Delta R_{ct}/R_{ct}$ value was calculated as follows:

$$\Delta R_{ct}/R_{ct} = \frac{(R_{ct,i+1} - R_{ct,i})}{R_{ct,i}}$$

where $R_{ct,i+1}$ and $R_{ct,i}$ are the electron transfer resistance before and after incubation with aptamer or HER2 (Bellagambi et al., 2017). The $(R_{ct,i+1} - R_{ct,i})/R_{ct,i}$ values for different aptasensors based on Hf-MOF, Zr-MOF, ZrHf-MOF, and CDs@ZrHf-MOF for detecting HER2 are illustrated in Fig. 2b. Although the Zr-MOF-based aptasensor exhibits a slightly higher aptamer immobilization ability ($\Delta R_{ct}/R_{ct}$ = 0.252) than that of Hf-MOF ($\Delta R_{ct}/R_{ct}$ = 0.202), the HER2 detection efficiency of Zr-MOF ($\Delta R_{ct}/R_{ct}$ = 0.181) seems more inferior. Since phosphoric groups in aptamer strands can be covalently bound with Zr(IV) centers of Zr-MOF by forming Zr-O-P bonds (Chen et al., 2016), the resulting conformation changes for aptamer strands become much difficult in the presence of this type of chemical bonds. It further results in the difficulty for HER2 to specifically bind with the aptamer strands, leading to the relatively lower detection sensitivity. Moreover, in comparison with Zr-MOF, Hf-MOF is more stable in aqueous solution since the bond dissociation energy of Hf-O (802 kJ mol^{-1}) is greater than that of Zr-O (776 kJ mol^{-1}) (SK et al., 2018), thus enhancing stability of the formed aptamer/HER2 complex. With respect to the bimetallic ZrHf-MOF, it displays a superior immobilization performance for aptamer strands but not a remarkable detection sensitivity for HER2. In case of the CDs@ZrHf-MOF-based aptasensor, the obvious improvements of both aptamer immobilization and HER2 detection is obtained. As aforementioned, the CDs was doped by the amino groups, thus enhancing the binding force of aptamers and improving the detection capability for HER2. Additionally, the existence of CDs can decline the crystallinity degree of ZrHf-MOF, as deduced by the XRD results. The increase of amorphous phase in the framework also can facilitate the biomolecule adsorption (Orellana-Tavra et al., 2015). In addition, the supramolecular interactions between MOFs and negatively charged nucleic acid sequences, including π-π stacking, hydrogen bonding and electrostatic force, can strengthen the anchor of aptamer strands (Su et al., 2017; Zhang et al., 2017a). Considering these comprehensive effect, including the interactions between aptamer strands and CDs@ZrHf-MOF (supramolecular interactions, Zr-O-P bonds, and electrostatic interactions between CDs and aptamers) and good electrochemical activity of CDs, the CDs@ZrHf-MOF-based biosensor shows the superior sensing performance to other ones. Thus, the CDs@ZrHf-MOF-based aptasensor was selected for the further sensitivity, selectivity, stability, reproducibility, and applicability measurements.

To obtain the optimal conditions for HER2 detection using the CDs@ZrHf-MOF-based aptasensor, the effect of binding time of HER2 and concentration for CDs@ZrHf-MOF suspension and aptamer solution, on the sensing performance was explored (See S7 in the Supplementary Information for details). The results reveal that the optimal conditions of the developed aptasensor are 5.0 mg mL^{-1} for CDs@ZrHf-MOF, 100 nM for aptamer solution, and 30 min for binding time of HER.

3.4. Detection limit of CDs@ZrHf-MOF-based aptasensor toward HER2

To evaluate the LOD of CDs@ZrHf-MOF-based aptasensor towards HER2, EIS measurements were carried out with different concentrations (0.1 pg mL^{-1}, 1 pg mL^{-1}, 0.01 ng mL^{-1}, 0.1 ng mL^{-1}, 1 ng mL^{-1}, 5 and 10 ng mL^{-1}) of HER2 in PBS (pH = 7.4) containing 5 mM $K_3[Fe(CN)_6]$/$K_4[Fe(CN)_6]$ (1:1) (Fig. 2**c**). It can be found that the R_{ct} values increase with increasing the HER2 concentration within the range of 0.1 pg mL^{-1} ~ 5 ng mL^{-1}. When the HER2 concentration is up to 10 ng mL^{-1}, the R_{ct} value reaches to a level off, indicating the achievement of equilibrium for the binding of aptamer and HER2. A good linearity can be calculated between the ΔR_{ct} value ($R_{ct,\ PTK7} - R_{ct,\ material}$) and the logarithm of HER2 concentration within a range of 0.1 pg mL^{-1} ~ 10 ng mL^{-1} (Fig. 2d), giving a regression equation ΔR_{ct} (kohm) = 1.303 + 0.997logC_{HER2} (ng mL^{-1}) with a correlation coefficient (R^2) of 0.997, where C_{HER2} is the concentration of HER2. The LOD of HER2 is calculated to be 30 fg mL^{-1}, of which LOD = 3σ/slope, where σ is the standard deviation of the blank measurement (Zhang et al., 2017b). Similarly, DPV was also used to evaluate the LOD of CDs@ZrHf-MOF-based aptasensor toward HER2 to reveal its performance (Figs. S14a and 14b), in which the regression equation of ΔI (μA) = 22.071 + 4.523 logC_{HER2} (ng mL^{-1}) (R^2 = 0.993) was obtained, showing a LOD of 19 fg mL^{-1}. Therefore, the consistent results of various electrochemical techniques confirm the sensing stability of the developed CDs@ZrHf-MOF-based aptasensor. All measurements were repeated for five times with relative standard deviations (RSD) less than 5%. Compared with other reported aptasensors for HER2 detection (Table 1), the CDs@ZrHf-MOF-based aptasensor shows excellent analytical performance with wider linear range and lower LOD. The excellent sensing performances of CDs@ZrHf-MOF-based aptasensor is mainly attributed to the following factors: (i) the phosphoric groups in aptamer strands are easily conjugated to the CDs@ZrHf-MOF via the strong Zr−O−P bonds (Chen et al., 2016); (ii) the high stability of the bimetallic MOF in aqueous solution can facilitate to enhance the stability of aptamer/HER2 complex (SK et al., 2018); (iii) the addition of amino-functionalized CDs can not only enhance the binding ability of aptamer strands but also boost the electrochemical activity of electrode (Wang et al., 2015).

3.5. Selectivity, stability, reproducibility and regenerability of CDs@ZrHf-MOF-based aptasensor toward HER2

The selectivity of the fabricated aptasensor was also investigated, in which HER2 was replaced by the possibly coexisting interfering proteins, such as vascular endothelial growth factor (VEGF), epidermal growth factor receptor (EGFR), prostate specific antigen (PSA), mouse immunoglobulin G (IgG), protein tyrosine kinase-7 (PTK7), carcino embryonic antigen (CEA), mucins 1 (MUC1) and their mixed solution at the same concentration of 0.01 ng mL^{-1} (100-fold concentration of HER2). It shows that the EIS response signal of interferences proteins is neglectable, while significant ΔR_{ct} responses are observed for the detection of HER2 and the mixed solution containing HER2 (Fig. 2e). This suggests the high selectivity of the

Table 1
Comparison of the proposed approach with other biosensors for HER2 detection.

Materials	Technique	Linear range (ng mL^{-1})	LOD	References
gold nanoparticle-based rolling circle amplification	Square wave voltammetry (SWV)	0.001–0.2	80 fg mL^{-1}	(Shen et al., 2018)
Ferrocene-labeled DNA/Au nanosphere	DPV	10–150	4.9 ng mL^{-1}	(Yang et al., 2018)
CuO nanoparticles	ELISA	0.025–5	0.956 pg mL^{-1}	(Tian et al., 2017)
Polycytosine DNA	SWV	0.001–1	0.5 pg mL^{-1}	(Li et al., 2018b)
Aptamer-based interdigitated electrode	EIS	0.1–10^4	0.1 ng mL^{-1}	(Arya et al., 2018)
Gold nanostructured screen-printed graphite	SPR	0–0.04	6.0 pg mL^{-1}	(Ravalli et al., 2015)
AntiHER2/APTMS-Fe_3O_4	DPV	0.0005–50	0.02 pg mL^{-1}	(Shamsipur et al., 2018)
CDs@ZrHf-MOF	EIS	0.0001–10	30 fg mL^{-1}	This work
	DPV	0.0001–10	19 fg mL^{-1}	

fabricated aptasensor for HER2 detection, which can be principally attributed to the specific binding between the targeting HER2 and aptamer (Qureshi et al., 2015).

In order to estimate the reproducibility of the aptasensor, the EIS responses of five aptasensors at a HER2 concentration of 0.1 pg mL^{-1} were measured independently (Fig. 2f). The RSD of 3.4% reveals a satisfactory reproducibility. Additionally, the long-term stability of the aptasensor is important in practical application. As shown in Fig. 2g, no obvious signal change is observed after 15 days, of which the signal remains ca. 108.5% of the original signal, also revealing the good stability of CDs@ZrHf-MOF-based aptasensor. The regenerability of the aptasensor was evaluated by immersing the HER2-bound electrode into 1.0 M NaOH at 4 °C for 10 min, which was washed with ultrapure water, and then used to detect HER2 again (0.1 pg mL^{-1}). Fig. 2h shows the R_{ct} values of the aptasensor during fifteen regeneration runs, where only a slight decrease for R_{ct} value is found, indicating that the aptasensor can be facilely regenerated. Consequently, the CDs@ZrHf-MOF-based aptasensor not only shows extremely low LOD for detecting HER2, but also illustrates high selectivity, good stability, excellent reproducibility, and well regenerability.

3.6. Application to human serum samples

To validate the potential applications of the developed aptasensor, the experiments were carried out by spiking HER2 of different concentrations (0.0001, 0.001, 0.01, 0.1, 1 and 5 ng mL^{-1}) into the human serum samples, which were detected directly without any pretreatments except for dilution with PBS (0.01 M). The results of HER2 determination in the human serum samples using the as-prepared aptasensor are summarized in Table S2. It is clear that the recoveries of serum samples are from 95.7% up to 108.3%, with a RSD lower than 3.7%. It hints that the CDs@ZrHf-MOF-based aptasensor can be used for HER2 detection in a complicated sample with the satisfied results.

3.7. Sensing performance of CDs@ZrHf-MOF-based aptasensor toward living MCF-7 cells

Based on the excellent biocompatibility of the as-prepared CDs@ZrHf-MOF and cell images (See S5 in the Supplementary Information), the fabricated aptasensor was also used for detecting the living MCF-7 cells by EIS (Fig. 3a). Obviously, the R_{ct} value was increased

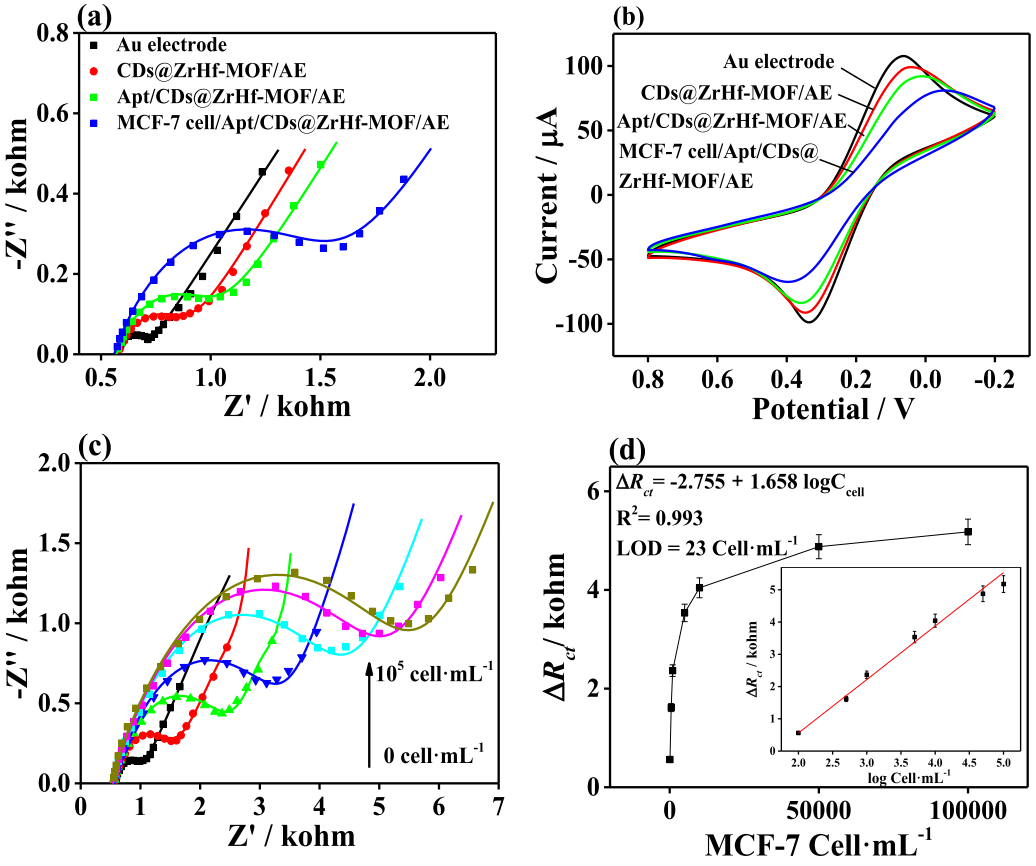

Fig. 3. (a) EIS Nyquist plots and (b) CV curves of CDs@ZrHf-MOF modified AEs for detection of MCF-7 cells in 0.1 M PBS (pH 7.4) containing 5.0 mM $[Fe(CN)_6]^{3-/4-}$ redox. (c) EIS responses of the CDs@ZrHf-MOF-based aptasensor with different MCF-7 cells concentrations (0, 1×10^2, 5×10^2, 1×10^3, 5×10^3, 1×10^4, 5×10^4, and 1×10^5 cells mL^{-1}). (d) Dependence of ΔR_{ct} on the concentration of MCF-7 cells (inset: the linear parts of calibration curves).

dramatically from 0.457 to 1.019 kohm when Apt/CDs@ZrHf-MOF/AE was used to detect living MCF-7 cells. It demonstrates that specific binding occurs between aptamer strands and the MCF-7 cells surfaces (Yan et al., 2019). Simultaneously, the CV results also show a good consistence with those of EIS (Fig. 3b). To assess the LOD of the fabricated aptasensors, MCF-7 cells with different concentrations (1×10^2, 5×10^2, 1×10^3, 5×10^3, 1×10^4, 5×10^4, and 1×10^5 cells mL^{-1}) were prepared for subsequent measurements. The R_{ct} values are increased with increasing the concentration of MCF-7 cells (Fig. 3**c**), giving a regression equation of ΔR_{ct} (kohm) = $-2.755 + 1.658 \log C_{cell}$ (cell·mL^{-1}) ($R^2 = 0.993$) and a LOD as low as 23 cells·mL^{-1}. As illustrated in Table S3, the sensing performance toward living MCF-7 cells of the aptasensor based on CDs@ZrHf-MOF outperforms those with other nanomaterials. This result is mainly originated from its excellent biocompatibility, high stability in aqueous solution, strong bioaffinity toward aptamer strands, and well intracellular endocytosis.

The selectivity of electrochemical biosensor was investigated by different interfering cells, such as L929 cells, and C6 cells. It demonstrates that L929 and C6 cells only show a relatively smaller R_{ct} value change (Fig. S15a), while EIS response of the MCF-7 cells exhibits substantial change. Additionally, to assess the reproducibility of biosensor, five electrodes were prepared for detecting the MCF-7 cells, giving a RSD of 4.6% (Fig. S15b). All these results demonstrate that the CDs@ZrHf-MOF-based aptasensor is highly selective with outstanding stability for the direct detection of the MCF-7 cells, hence showing a considerable potential for clinical applications.

4. Conclusion

In summary, a novel nanocomposite CDs@ZrHf-MOF was designed and synthesized by embedding the amino-functionalized CDs into bimetallic ZrHf-MOF, leading to good electrochemical activity, excellent biocompatibility and defective nanostructure. The strong binding of aptamer strands endows the CDs@ZrHf-MOF-based aptasensor with high detecting sensitivity toward HER2 and MCF-7 cells. Notably, the synergistic effect of CDs, Zr-MOF, and Hf-MOF can not only facilitate the enhancement of electrochemical activity but also improve the stability of the formed G-quadruplex between the aptamer strands and HER2. As such, the CDs@ZrHf-MOF-based aptasensor shows an extremely LOD of 19 fg mL^{-1} and 23 cell mL^{-1} toward HER2 and MCF-7 cells, respectively, along with good selectivity, stability, reproducibility, and acceptable applicability. Though the validation of this aptasensor can be revealed using human serum samples, its application needs to be further evaluated in future using the real time clinical specimens.

CRediT authorship contribution statement

Chenxi Gu: Validation, Formal analysis, Writing - original draft. **Chuanpan Guo:** Methodology, Formal analysis, Investigation. **Zhenzhen Li:** Methodology, Investigation. **Minghua Wang:** Visualization. **Nan Zhou:** Writing - review & editing. **Linghao He:** Formal analysis, Validation. **Zhihong Zhang:** Conceptualization, Writing - review & editing, Supervision. **Miao Du:** Formal analysis, Writing - review & editing.

Acknowledgements

This work was supported by the National Natural Science Foundation of China (Nos. U1604127, U1704256, and 81601082), Innovative Technology Team of Henan Province (No. CXTD2014042), and the Key Research Project of University of Henan Province (No. 19zx004).

Declaration of interest statement

We declare that we have no conflict of interest.

Appendix A. Supporting information

Supplementary data associated with this article can be found in the online version at doi:10.1016/j.bios.2019.03.043.

References

Arkan, E., Saber, R., Karimi, Z., Shamsipur, M., 2015. Anal. Chim. Acta 874, 66–74.
Arya, S.K., Zhurauski, P., Jolly, P., Batistuti, M.R., Mulato, M., Estrela, P., 2018. Biosens. Bioelectron. 102, 106–112.
Bagheri, H., Ranjbari, E., Amiri-Aref, M., Hajian, A., Ardakani, Y.H., Amidi, S., 2016. Biosens. Bioelectron. 85, 814–821.
Bala, R., Kumar, M., Bansal, K., Sharma, R.K., Wangoo, N., 2016. Biosens. Bioelectron. 85, 445–449.
Bellagambi, F.G., Baraket, A., Longo, A., Vatteroni, M., Zine, N., Bausells, J., Fuoco, R., Di Francesco, F., Salvo, P., Karanasiou, G.S., Fotiadis, D.I., Menciassi, A., Errachid, A., 2017. Sens. Actuators B-Chem. 251, 1026–1033.
Bethune, G.C., Veldhuijzen Van Zanten, D., MacIntosh, R.F., Rayson, D., Younis, T., Thompson, K., Barnes, P.J., 2015. Histopathology 67, 880–887.
Chen, L., Ou, J., Wang, H., Liu, Z., Ye, M., Zou, H., 2016. ACS Appl. Mater. Interfaces 8, 20292–20300.
Chinen, A.B., Guan, C.M., Ferrer, J.R., Barnaby, S.N., Merkel, T.J., Mirkin, C.A., 2015. Chem. Rev. 115, 10530–10574.
DeSantis, C.E., Bray, F., Ferlay, J., Lortet-Tieulent, J., Anderson, B.O., Jemal, A., 2015. Cancer Epidem. Biomar. 10.
Dong, H., Chen, H., Jiang, J., Zhang, H., Cai, C., Shen, Q., 2018. Anal. Chem. 90, 4507–4513.
Du, M., Li, C., Liu, C., Fang, S., 2013. Coord. Chem. Rev. 257, 1282–1305.
Duan, D., Yang, H., Ding, Y., Ye, D., Li, L., Ma, G., 2018. Electrochim. Acta 261, 160–166.
Emami, M., Shamsipur, M., Saber, R., Irajirad, R., 2014. Analyst 139, 2858–2866.
Falcaro, P., Ricco, R., Yazdi, A., Imaz, I., Furukawa, S., Maspoch, D., Ameloot, R., Evans, J.D., Doonan, C.J., 2016. Coord. Chem. Rev. 307, 237–254.
Feng, J., Liu, J., Wu, B., Wang, G., 2010. Anal. Chem. 82, 4520–4528.
Furrer, D., Sanschagrin, F., Jacob, S., Diorio, C., 2015. Am. J. Clin. Pathol. 144, 686–703.
Golabi, M., Kuralay, F., Jager, E.W.H., Beni, V., Turner, A.P.F., 2017. Biosens. Bioelectron. 93, 87–93.
Guo, C., Su, F., Song, Y., Hu, B., Wang, M., He, L., Peng, D., Zhang, Z., 2017. ACS Appl. Mater. Inter. 9, 41188–41199.
Ilkhani, H., Farhad, S., 2018. Anal. Biochem. 557, 151–155.
Ilkhani, H., Ravalli, A., Marrazza, G., 2016. Design of an Affibody-Based Recognition Strategy for Human Epidermal Growth Factor Receptor 2 (HER2) Detection by Electrochemical Biosensors., 23.
Ilkhani, H., Sarparast, M., Noori, A., Zahra Bathaie, S., Mousavi, M.F., 2015. Biosens. Bioelectron. 74, 491–497.
Ju, J., Chen, W., 2015. Anal. Chem. 87, 1903–1910.
Li, C., Wu, R., Zou, J., Zhang, T., Zhang, S., Zhang, Z., Hu, X., Yan, Y., Ling, X., 2018a. Biosens. Bioelectron. 116, 81–88.
Li, X., Shen, C., Yang, M., Rasooly, A., 2018b. Anal. Chem. 90, 4764–4769.
Liu, C., Sun, C., Tian, J., Wang, Z., Ji, H., Song, Y., Zhang, S., Zhang, Z., He, L., Du, M., 2017a. Biosens. Bioelectron. 91, 804–810.
Liu, C., Zhang, Z., Chen, M., Zhao, H., Duan, F., Chen, D., Wang, M., Zhang, S., Du, M., 2017b. Chem. Commun. 53, 3941–3944.
Liu, Y., Hou, W., Xia, L., Cui, C., Wan, S., Jiang, Y., Yang, Y., Wu, Q., Qiu, L., Tan, W., 2018. Chem. Sci. 9, 7505–7509.
Morris, W., Briley, W.E., Auyeung, E., Cabezas, M.D., Mirkin, C.A., 2014. J. Am. Chem. Soc. 136, 7261–7264.
Morris, W., Wang, S., Cho, D., Auyeung, E., Li, P., Farha, O.K., Mirkin, C.A., 2017. ACS Appl. Mater. Inter. 9, 33413–33418.
Niazi, J.H., Verma, S.K., Niazi, S., Qureshi, A., 2015. Analyst 140, 243–249.
Orellana-Tavra, C., Baxter, E.F., Tian, T., Bennett, T.D., Slater, N.K.H., Cheetham, A.K., Fairen-Jimenez, D., 2015. Chem. Commun. 51, 13878–13881.
Pan, Y., Zhan, S., Xia, F., 2018. Anal. Biochem. 546, 5–9.
Qureshi, A., Gurbuz, Y., Niazi, J.H., 2015. Sens. Actuators B-Chem. 220, 1145–1151.
Ravalli, A., Da Rocha, C.G., Yamanaka, H., Marrazza, G., 2015. Bioelectrochemistry 106, 268–275.
Ravalli, A., Voccia, D., Palchetti, I., Marrazza, G., 2016. Biosensors 6, 39.
Shamsipur, M., Emami, M., Farzin, L., Saber, R., 2018. Biosens. Bioelectron. 103, 54–61.
Shan, G., Huang, H., Deng, X., Chen, Y., Jiang, Z., Min, X., Liu, S., Huang, W., Xiang, Z., 2018. Nano Res. 1–13.
Shao, K., Wang, B., Nie, A., Ye, S., Ma, J., Li, Z., Lv, Z., Han, H., 2018. Biosens. Bioelectron. 118, 160–166.
Shen, C., Liu, S., Li, X., Zhao, D., Yang, M., 2018. Microchim. Acta 185, 547.
SK, M., Nandi, S., Singh, R.K., Trivedi, V., Biswas, S., 2018. Inorg. Chem. 57, 10128–10136.
Su, F., Zhang, S., Ji, H., Zhao, H., Tian, J., Liu, C., Zhang, Z., Fang, S., Zhu, X., Du, M., 2017. ACS Sens. 2, 998–1005.
Tabasi, A., Noorbakhsh, A., Sharifi, E., 2017. Biosens. Bioelectron. 95, 117–123.
Takata, T., Pan, C., Nakabayashi, M., Shibata, N., Domen, K., 2015. J. Am. Chem. Soc.

137, 9627–9634.
Téllez-Plancarte, A., Haro-Poniatowski, E., Picquart, M., Morales-Méndez, G.J., Lara-Cruz, C., Jiménez-Salazar, E.J., Damián-Matsumura, P., Escobar-Alarcón, L., Batina, N., 2018. Nanomaterials 8, 549.
Tian, S., Zeng, K., Yang, A., Wang, Q., Yang, M., 2017. J. Immunol. Methods 451, 78–82.
Toh, S.Y., Citartan, M., Gopinath, S.C.B., Tang, T., 2015. Biosens. Bioelectron. 64, 392–403.
Tuteja, S.K., Chen, R., Kukkar, M., Song, C.K., Mutreja, R., Singh, S., Paul, A.K., Lee, H., Kim, K., Deep, A., Suri, C.R., 2016. Biosens. Bioelectron. 86, 548–556.
Vermoortele, F., Bueken, B., Le Bars, G., Van de Voorde, B., Vandichel, M., Houthoofd, K., Vimont, A., Daturi, M., Waroquier, M., Van Speybroeck, V., Kirschhock, C., De Vos, D.E.,, 2013. J. Am. Chem. Soc. 135, 11465–11468.
Vivek, R., Thangam, R., NipunBabu, V., Rejeeth, C., Sivasubramanian, S., Gunasekaran, P., Muthuchelian, K., Kannan, S., 2014. ACS Appl. Mater. Interfaces 6, 6469–6480.
Wang, C., Qian, J., Wang, K., Hua, M., Liu, Q., Hao, N., You, T., Huang, X., 2015. ACS Appl. Mater. Inter. 7, 26865–26873.
Wang, M., Yang, L., Hu, B., Liu, J., He, L., Jia, Q., Song, Y., Zhang, Z., 2018b. Biosens. Bioelectron. 113, 16–24.
Wang, S., Li, Z., Duan, F., Hu, B., He, L., Wang, M., Zhou, N., Jia, Q., Zhang, Z., 2019. Anal. Chim. Acta 1047, 150–162.
Wang, Z., Dong, P., Sun, Z., Sun, C., Bu, H., Han, J., Chen, S., Xie, G., 2018a. J. Mater. Chem. B 6, 2426–2431.
Yan, X., Song, Y., Liu, J., Zhou, N., Zhang, C., He, L., Zhang, Z., Liu, Z., 2019. Biosens. Bioelectron. 126, 734–742.
Yang, S., You, M., Zhang, F., Wang, Q., He, P., 2018. Sens. Actuators B-Chem. 258, 796–802.
Ye, X., Shi, H., He, X., Wang, K., He, D., Yan, L.A., Xu, F., Lei, Y., Tang, J., Yu, Y., 2015. Anal. Chem. 87, 7141–7147.
Zhang, Y., Xiao, J., Sun, Y., Wang, L., Dong, X., Ren, J., He, W., Xiao, F., 2018. Biosens. Bioelectron. 100, 453–461.
Zhang, Z., Duan, F., Tian, J., He, J., Yang, L., Zhao, H., Zhang, S., Liu, C., He, L., Chen, M., Chen, D., Du, M., 2017a. ACS Sens. 2, 982–989.
Zhang, Z., Guo, C., Zhang, S., He, L., Wang, M., Peng, D., Tian, J., Fang, S., 2017b. Biosens. Bioelectron. 89, 735–742.
Zhang, Z., Zhai, S., Wang, M., He, L., Peng, D., Liu, S., Yang, Y., Fang, S., Zhang, H., 2015. Anal. Methods-UK 7, 4725–4733.
Zhao, D., Wan, X., Song, H., Hao, L., Su, Y., Lv, Y., 2014. Sens. Actuators B-Chem. 197, 50–57.
Zhou, H.J., Kitagawa, S., 2014. Chem. Soc. Rev. 43, 5415–5418.
Zhou, N., Su, F., Li, Z., Yan, X., Zhang, C., Hu, B., He, L., Wang, M., Zhang, Z., 2019. Microchim. Acta 186, 10–1007.
Zhou, N., Yang, L., Hu, B., Song, Y., He, L., Chen, W., Zhang, Z., Liu, Z., Lu, S., 2018. Anal. Chem. 90, 13624–13631.